The paper was published in the proceedings of the 20th International Conference on Soil Mechanics and Geotechnical Engineering and was edited by Mizanur Rahman and Mark Jaksa. The conference was held from May 1st to May 5th 2022 in Sydney, Australia.

Proceedings of the 20th International Conference on Soil Mechanics and Geotechnical Engineering– Rahman and Jaksa (Eds)
© 2022 Australian Geomechanics Society, Sydney, Australia, ISBN 978-0-9946261-4-1

Visualization testing system of spatial deformation based on transparent soil and 3D reconstruction technology

Honghua Zhao
Department of Engineering Mechanics, Dalian University of Technology, P.R. China, zhaoh@dlut.edu.cn

Cong Liu & Xiaowei Tang
School of Civil Engineering, Dalian University of Technology, P.R. China, zhaoh@dlut.edu.cn

Huanwei Wei
School of Civil Engineering, Shandong Jianzhu University, P.R. China

ABSTRACT: This paper presents a developing novel automatic tomographic scanning measuring device using two sets of high-precision motorized linear stages, combining the synchronization control system of both laser device and CCD industrial camera. Based on the developed tomographic scanning measuring device, visualization of spatial deformation behaviour around a penetrating pile in sand was investigated quantitatively using transparent soil and incremental reliability-guided particle image velocimetry technique, with the aid of a modified 3D reconstruction technique. Model pile penetration tests on a saturated transparent soil sample were carried out under a constant rate of penetration. The spatial deformation pattern of different pile types around a penetrating pile was discussed. In addition, the spatial disturbance effect caused by different penetration stages was also discussed herein. The test results showed that the developed novel automatic tomographic scanning measuring device with the modified 3D reconstruction procedure could be an innovative tool in geotechnical physical model experiments.

KEYWORDS: tomographic scanning; 3D reconstruction; spatial deformation; calibration tests; transparent soil; pile penetration

1 INTRODUCTION

The penetration mechanism of a jacked pile, and the disturbance effect on the soil during penetration, which has enjoyed a significant surge of attention in the last 20 years (Hwang et al. 2001, Yetginer et al. 2006, Salgado & Prezzi 2007, Randolph & Wroth 2010). Comprehensive full-scale test, a 'half-model' chamber test and centrifuge model test have been used to capture stresses and displacements in soil around a penetration pile (Paniaguaetal et al. 2013, White & Bolton 2004, Hu et al. 2015). Though these studies are valuable for understanding the mechanisms of pile-soil interactions, the experiments are limited by influence of intrusive transducers on deformation monitoring and the inability to reveal the full-field true displacement.

In recent years, many research efforts have been devoted to the development of non-destructive three-dimensional (3D) deformation measurement technology. Typically, stereo particle image velocimetry (stereo-PIV) was a more advanced optical measurement method based on the PIV technique and a binocular vision model. Two cameras capture images from different angles, then the 3D displacement field was calculated using the paired images and reconstruct algorithm (Yuan et al. 2013, 2015, Garcia et al. 2002, Scarano 2013). Recently, in order to reduce hardware investment and eliminate the need of precise camera synchronization, single-camera stereo-PIV technique was realized by placing an additional optical device (Yu & Pan 2017). However, thus far, the stereo-PIV technique could only provide three-dimensional surface information. Additionally, the use of advanced non-intrusive techniques, such as X-ray computed tomography (CT) scanning and magnetic resonance imaging, in geotechnical small-scale model have been applied to produce visual images for not only in cross section but also the images in 3D (Hall et al. 2010, Higo et al. 2012, Viggiani et al. 2015). Nevertheless, routine application of these techniques was limited by their high costs and small experimental operation space. Transparent soil combined with PIV processing technique was introduced in order to overcome the opaque nature of soil for measuring spatial deformations. However, most of these studies were revealing two-dimensional plane problems (Ni et al. 2010, Hird et al. 2011, Kong et al. 2015, Xiao et al. 2016, Zhao et al. 2018). Limited case studies of measuring three-dimensional spatial deformations within a transparent soil model were reported (Toiya et al. 2007, Iskander & Liu 2010, Losert et al. 2009, Cataldo et al. 2017).

The present paper describes a penetration experiment of jacked pile in a novel automatic tomographic scanning measuring device combining transparent soil model with increment reliability-guided particle image velocimetry technique (increment RG-PIV). The developed automatic tomographic scanning measuring device can properly obtain the spatial deformation inside the soil. A modified 3D reconstruction technique is proposed, by which the disturbance effect of pile penetration is successfully quantified. The results demonstrate that this new measuring method has potential for contributing to the understanding of penetration mechanisms and spatial displacement patterns for the penetration problem of a static pressure pile. Furthermore, it opens up new possibilities for revealing underlying physics and guiding geotechnical problems.

2 EXPERIMENTAL SET-UP AND METHOD

2.1 *Transparent soil model*

Transparent soils are two-phase media made by refractive index (RI) matching of solids representing the soil skeleton and the saturating fluids (Iskander et al 2015). The granular material used in this experiment was fused quartz, which was manufactured by through melting the quartz at high temperature. in China. In order to simulate sandy soil, the grain size of the fused quartz is in the range of 0.1-2 mm. The grain size distribution curve for the fused quartz is shown in Figure 1. Fused quartz has a specific gravity of 2.33, and a drained friction angle in the range of 38.6°- 40.3°. More details regarding physical properties of fused quartz can be found in Table 1. The mixed pore fluid comprised of nParaffin C12 and White Oil 15 at a volume ratio of 1:4.75. The magnetic agitator (Fig.2a) was used to fully stir the two immiscible liquids, and the refraction index (RI) of the mixed pore liquid was 1.4590 at 20.0°C, which is the same refractive index as the reported RI of fused quartz (Zhao & Ge, 2014; Sang et al., 2019).

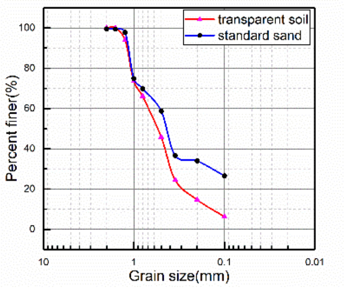

Figure 1 Grain size distribution curve for the fused quartz and Fu jian (China) standard sand.

Table 1. Basic properties of fused quartz

C_u	C_c	ρ_d (g/cm^3)	ρ_{dmax} (g/cm^3)	ρ_{dmin} (g/cm^3)	D_r (%)
5.14	1.51	1.4	1.56	1.18	65

C_u : coefficient of ununiformity; C_c : coefficient of curvature.

For the sample preparation of transparent soils, the fused quartz particles are first cleaned with distilled water and then dried in the electric thermostatic drier box. After then, fused quartz particles were placed in a model box made of glass with a dimension of 300mm×180mm×280 mm (length×width×height) by pluviating using a funnel. In order to prevent the occurrence of stratification, it is necessary to mix and compact the filled fused quartz. Then, insert the hose into the bottom of the model box and slowly fill the model box with pore fluid from the bottom up. For the transparent soil sample, the height of this pore fluid must be higher than the surface of this fused quartz 20mm in order to filter the air entering during the pile model penetration. Afterward, a vacuum pump was applied to de-air the transparent soil sample. The saturated transparent soil sample is consolidated through the loading system by means of the pre-drilled organic glass plate. The transparent soils sample has excellent transparency as illustrated in Figure 2.

In the pile penetration tests, the model piles were made of polymethyl methacrylate, as shown in Fig.2b. The length of the piles was about 125 mm, with a diameter of 22 mm. In order to minimize reflection of light, the surface of all piles are roughened, which provides consistent friction conditions for the model test and gives full play to the interaction between the pile and the soil.

2.2 *Automatic tomographic scanning measuring device and experimental setup*

In order to visualize the three-dimensional spatial deformation of pile penetration problem, a high-precision motorized linear stages with a scientific grade CCD camera and a laser scanning illumination system is employed. Figure 3 illustrates the custom experimental setup of novel automatic tomographic scanning measuring. It includes an axial loading subsystem and two measuring subsystem. The measuring subsystem is mainly composed of a laser transmitter, a CCD camera, a computer, a set of image acquisition software, two sets of high-precision motorized linear stages: one for the laser device and one for the CCD camera. The two sets of high-precision motorized linear stages are composed of a stepper motor, a couplings, a ball screw, a small size rail and grating ruler. In image collection, the CCD camera and the laser device move the same distance synchronously to obtain a two-dimensional (2D) image at different locations, and the closed-loop control system is used to ensure high synchronization control accuracy. By referring to the idea of 3D reconstruction of CT scan in medical science, a 3D reconstruction method is used to quantitatively calculate 3D deformation field from a series of deformed 2D images at different positions.

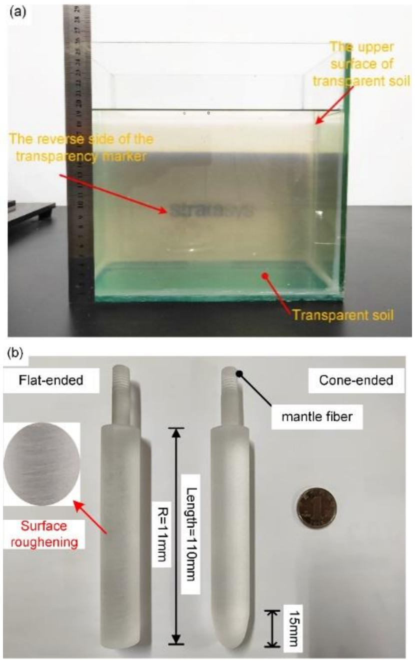

Figure 2a Reference viewed behind a 18cm thick model made of transparent soil. 2b Two types of the small scale pile models.

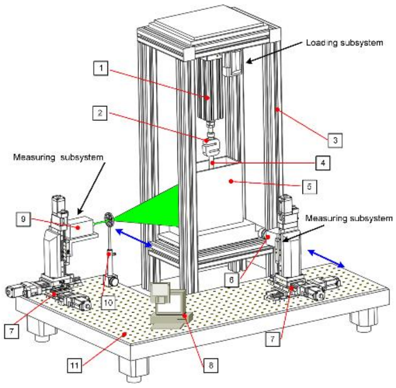

Figure 3 Schematic diagram of experimental setup :(1) Electric servo cylinder, (2) Load cell, (3) Loading frame, (4) Model pile, (5) Transparent soil model box, (6) CCD industrial camera, (7) High-precision motorized linear stages, (8) Computer, (9) Laser device, (10) Optical prism, (11) Optical platform.

2.3 *Incremental reliability-guided particle image velocimetry method*

White (2003) reported that particle image velocimetry (PIV) image processing technology was used as a method to measure soil deformation in geotechnical model tests. Since then, PIV technique has become routine experimental practice to obtain deformation patterns in many geotechnical research laboratories (Iskander et al 2010, Stanier et al 2015). An important step in

PIV technique is to track the deformation information between consecutive speckle images taken before and after deformation. This step first selects seed point in the reference image and defines the target image, and then each image is partitioned into many smaller areas called subsets. Each subset of 2N×2N pixels corresponds to one seed point in each image. The similarity between reference subset and target subset is evaluated according to the correlation criterion. The seed points in the target image can be located through searching the peak location of the distribution of correlation coefficients. With the aid of the camera calibration parameter (the scale ratio of the object space coordinates to the pixel coordinates), the pixel differences of the location of the reference subset center and the target subset center yield the displacement vector at seed point (Pan et al. 2012). To determine the corresponding location of each subset in the deformed image, various correlation functions are defined, such as Cross-Correlation (CC), Sum of Absolute Differences (SAD) (Vanne et al. 2006) and Zero-mean Normalized Sum of Squared Difference (ZNSSD). Generally speaking, the ZNSSD is insensitive to the scale and offset changes in illumination lighting fluctuations, which is highly recommended to use among the many correlation criterion. The ZNSSD criterion can be defined as:

$$C_{ZNSSD}(p) = \sum\sum\left[\frac{f(x,y)-f_m}{\sqrt{\sum\sum[f(x,y)-f_m]^2}} - \frac{g(x',y')-g_m}{\sqrt{\sum\sum[g(x'-y')-g_m]^2}}\right]^2 \qquad (1)$$

where $f(x,y)$ is the grayscale value at coordinates (x,y) in the reference subset of the reference image and g(x',y') is the grayscale value at coordinates (x',y') in the target subset of the deformed image; f_m and g_m are mean values of grayscale intensity of reference and target subsets, respectively (Pan et al. 2007, 2010).

Currently, the most effective pattern-recognition algorithm is incremental reliability-guided digital image correlation (RG-PIV), which is based on ZNSSD of the grayscale intensity characteristics between consecutive speckle images taken before and after deformation (Pan et al 2012). In RG-PIV algorithm, some initial seed points are defined in the original reference image and tracked its corresponding locations in a series of deformed images. If the computed correlation coefficient of initial seed points in a series of image are smaller than predefined threshold, which means no decorrelation effect exists in the deformed image, the predefined reference image is employed to continue correlation analysis. However, if the ZNSSD of the current deformed image is larger than the predefined threshold, the image recorded just before the current deformed image is selected as an updated reference image to continue correlation analysis (Pan et al 2012). With the aid of the idea of incremental RG-PIV, the image post-processing program in this paper is an improved program based on the existing MatPIV program with the method of automatically updating the reference image. Considering that the penetration problem of jacked piles is a three-dimensional large deformation with out-of-plane displacement, the predefined threshold of the ZNSSD coefficient is set to be 0.6 (1 is completely correlated, 0 is completely irrelevant).

2.4 *Image processing and 3D reconstruction method*

Three-dimensional reconstruction method is a new technology which can obtain 3D images and measure them quantitatively by means of post-processing a series of continuous images with computer software (Cnudde & Boone 2012, Zhang et al. 2014, Kashuk et al. 2015). An important challenge in 3D reconstruction is how to build a 3D model from a series of 2D slices information. In order to obtain accurate 2D speckle image information, incremental RG-PIV algorithm was used in image post-processing (Pan et al. 2012). The newly developed 3D reconstruction method is volume rendering method (Zheng 2016). Firstly, the 2D images of sequence was obtained by the tomographic scanning measuring device. The deformation data of 24 slice positions were calculated by the incremental RG-PIV algorithm, and the coordinates and deformation data of 24 slice positions were extracted by MATLAB. Then the discrete 3D volume data matrix (x, y, z, data) was constructed. Subsequently, the cubic spline interpolation function is used to obtain the missing data between the two slices in order, and then the experimental data and the interpolated data are integrated into a complete 3D volume data matrix. The construction principle of 3D data set is shown in Figure 4. After constructing the data set, the image information is smoothed, filtered, grayscale transformation and equalization processing by using the toolbox in MATLAB. Then, volume rendering method is used to project the 3D data field. To accurately reflect the spatial details, the well-developed Ray Casting algorithm is used to map the planar projection (Cubes 1987, Levoy 1988). Subsequently, the three-dimensional image fragments are constructed and the normal direction of the fragments are calculated. Finally, the ideal 3D reconstruction image is shown.

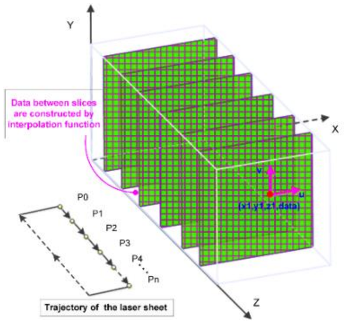

Figure 4 Construction of three-dimensional data set

3 RESULTS AND ANALYSIS

The series of 2D speckle images about pile penetrating model tests obtained through the automatic tomographic scanning measuring device were shown in Figure 5. As can be seen from Figure 5, the first slice is at the axial section of the model pile, and the remaining slices extend outward along the Y-axis with fixed spacing.

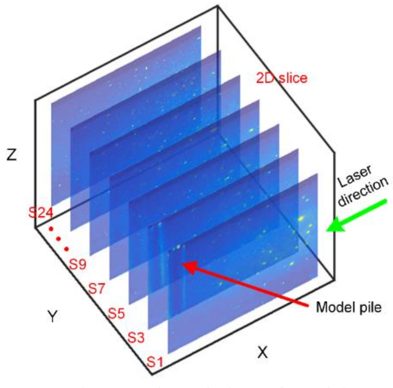

Figure 5 The actual rendering of model tests

3.1 *Comparison of the displacement pattern between flat-ended pile and cone-ended pile*

Figure 6 presents the penetration depth-time curve and the penetration resistance-time curves for flat-ended pile and cone-ended pile. As the display of the penetration depth-time curve indicated, the model pile penetration test adopts displacement control method. For each penetration state, the penetration depth is 0.5R, and then the slices at all positions are scanned during image acquisition. Comparing the penetration resistance-time curves of flat-ended pile and cone-ended pile, the penetration resistance of flat-ended pile is always greater than that of cone-ended pile. For each penetration cycle: the penetration resistance gradually increases during the penetration phase; the penetration resistance decreases instantaneously during the image acquisition phase, and then slowly decrease. This is because during the penetration phase, the pile tip is subjected to continuous penetration resistance, and the pile has the same speed as the soil under the pile tip. When the pile stops penetrating, the pressing effect of the pile on the soil is no longer enhanced. At the same time, due to the inertia effect, the soil under the pile tip moves further downward. Therefore, the penetration resistance decreases instantaneously. However, because the soil mass at the bottom of the pile tip is in a state of high stress, the compression effect on the surrounding soil mass due to the penetration test of the static pile will not dissipate quickly. At the same time, because the interval of image acquisition is short, the change trend of penetration resistance decreases suddenly and then slowly. Regarding the relationship between penetration resistance and penetration depth, a similar trend was observed by Iskander & Liu (2010). For the penetration resistance-time curve of cone-ended pile, the penetration resistance was zero at the initial stage of the penetration process. However, the penetration resistance is zero for a short time. When the pile penetrates to the depth of 1R, the penetration resistance gradually increases. This is possibly due to that the sandy soil has no cohesive force, the surface soil cannot withstand the pressure. Although the surface of the model pile is rough, the contact area between the pile tip and the soil is small for the cone-ended pile at the initial stage of penetration. In addition, the penetration form of cone-ended pile is punching into the soil, which is different from the form of squeezing soil of flat-ended pile. In the initial stage of penetration, the confining pressure on the upper soil is small and the restriction effect on the soil around the pile tip is small, so the penetration resistance of the cone-ended pile is almost zero. However, for the penetration resistance-time curve of flat-ended pile, due to the large contact area between pile tip and soil, the pile tip is subject to penetration resistance at the initial stage of the penetration process.

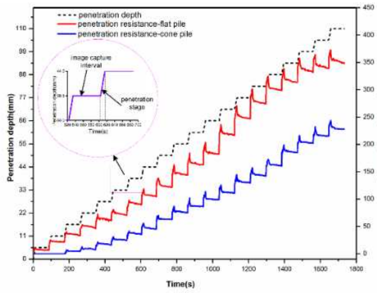

Figure 6 The penetration depth-time and the penetration resistance-time curves

In order to improve the understanding of the different penetration mechanism of the two types of piles, the spatial displacement fields for flat-ended pile and cone-ended pile are compared in Figure 7, 8 and 9. To quantify and display the differences of soil movement, the isosurface of displacement normalized by pile radius R. Outward and downward movements are labelled as positive, and inward and upward movements as negative. Figure 7a exhibited that the front view of spatial vertical displacement isosurface for flat-ended pile penetration when the pile penetrates to the depth of 10R. It can be seen that the spatial vertical displacement isosurface can be roughly divided into two parts: compression region at the bottom of pile tip and uplifted region around pile body. For the uplifted region, the vertical displacement decreases radially in the radial direction. Regarding the compression region, it is shaped like a light bulb with the maximum vertical displacement at the center of the bulb (Ni et al. 2010, Chong 2013 Kobayashi & Fukagawa 2003, Massarsch & Wersall 2013). The height of the bulb is approximately 5R, and the width of the bulb is about 4R. Thus, this means that the high pressure stressing zone during the continuous penetration extends roughly outward within the range of 4R. Figure 7b shows the side view of spatial vertical displacement isosurface for flat-ended pile. The vertical displacement value of 0.02R is taken as the standard to quantify the maximum influence range of soil disturbance, and the influence range of flat-ended pile penetration on the surrounding soil disturbance is 13.6R.

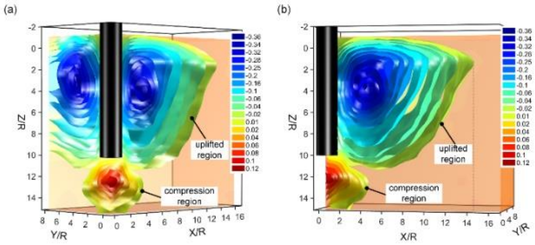

Figure 7 The spatial vertical displacement isosurface of flat-ended pile penetration, δw/R: a front view; b side view.

Figure8a, 8b show the front view and the side view of spatial vertical displacement isosurface for the cone-ended pile penetration when the pile penetrates to the depth of 10R, respectively. The vertical displacement of flat-ended pile penetration is greater than that of cone-ended pile penetration. It was observed that there is general agreement between flat-ended pile and cone-ended pile for the spatial vertical displacement contour. Nevertheless, there is a significant difference in the compression region: the direction of the isosurface of the vertical displacement at the bottom of cone-ended pile is approximately along the normal direction of the conical plane. This is attributed to the reason that the cone-ended pile penetration is mainly through the pile tip punching into the soil, and continuous shearing process occurs between the pile and soil along the cone surface, pushing the soil to the two sides.

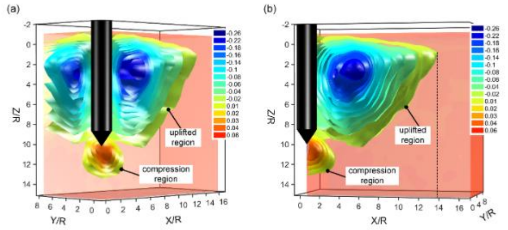

Figure 8 The spatial vertical displacement isosurface of cone-ended pile penetration, δw/R: a front view; b side view.

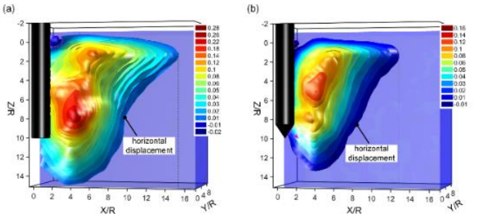

Figure 9 The spatial horizontal displacement isosurface, δu/R: a flat-ended pile; b cone-ended pile.

Note that the spatial horizontal displacement isosurface for flat-ended pile and cone-ended pile when the pile penetrates to the depth of 10R as indicated in Figure 9a, 9b. Regarding the influence of pile penetration on the surrounding soil disturbance, the spatial horizontal displacement trend is similar for flat-ended pile and cone-ended pile. The horizontal displacement is caused by the lateral expansion in the process of pile penetration. The lateral expansion can be roughly divided into two stages: when the pile tip contacted the soil, the soil disturbance around the pile tip will produce a compressive expansion effect; when the pile tip has passed, it has the effect of secondary accumulation expansion on the upper soil. Due to the friction force between the surface of pile shaft and soil, a small part of negative horizontal displacement area appears near the upper surface of pile in Figure.

The horizontal displacement of flat-ended pile penetration is greater than that of cone-ended pile penetration. The horizontal displacement value of 0.01R is taken as the standard to quantify the maximum influence range of soil disturbance, the influence range of flat-ended pile and cone-ended pile penetration on surrounding soil disturbance is 14.3R, 11.8R, respectively.

Figure 10a, 10b displays the spatial displacement vector field for the flat-ended pile and the cone-ended pile when the pile penetrates to the depth of 10R. In the case of a shallow penetration (the penetration depth of the pile is less than 10 times the pile diameter), it can be observed that the direction of the vector arrow on the outside of the pile is inclined upward, and there are a few downward arrows at the bottom of the pile, which further verifies that the deformation of soil around the pile is mainly inclined upward for the so-called shallow penetration (Cooke et al. 1979). Meanwhile, the angle between the motion direction of the vector arrow and the X-axis for slice far from the pile is greater than that of slice near the pile. Comparing Figure 10a with 10b, it can be concluded that the size and influence range of displacement vector for flat-ended pile penetration are larger than that of the cone-ended pile penetration. Considering the vector field pattern surrounding the pile tip, the vector direction at the bottom of the pile tip is initially vertical downward, then the vector direction of the soil in the transition zone gradually rotate toward oblique upward, resulting in oblique upward movement of displacement vectors on one side of the penetrating pile (Massarsch & Wersall 2013). This is because the process of pile penetration is a cavity expansion process, and soil particle will undergo the resistance caused by passive earth pressure in the process of movement. Since the upper confining pressure is less than the lateral confining pressure, the soil particle will move upward.

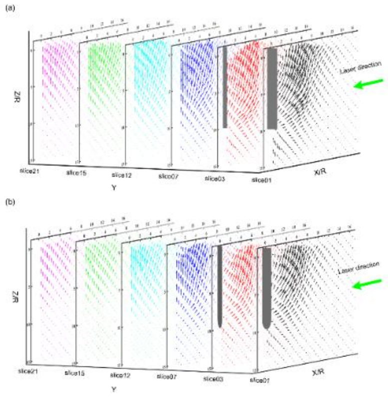

Figure 10 The spatial displacement vector field: a flat-ended pile; b cone-ended pile.

3.2 *Deformation behaviour during continuous penetration*

Regarding the different stages of vertical displacement for flat-ended pile penetration, a systematic comparison for penetration depth of 3.5R, 7R, 10R in Figure 11. It is shown that the variation trend of vertical displacement in different stages is similar. As the penetration depth increases gradually, the vertical displacement increases gradually, and the influence range on the surrounding soil disturbance increases gradually. For the compression region, when the penetration depth increases from 3.5R to 7R, the vertical displacement and influence range of the compression region become larger. However, when the penetration depth increases from 7R to 10R, the vertical displacement is generally in a stable trend, but the influence range on the surrounding soil disturbance gradually increases.

Examples of the surface heave of different stages for flat-ended pile penetration is shown in Figure 12 obtained from the measured displacement data. It can be observed that the variation trend of ground heave is roughly similar in different penetration stages, which increases first and then decreases. With the increase of penetration depth, the position of the maximum ground heave gradually moves away from the pile shaft. At the same time, with the increase of penetration depth, the ground heave and influence range are gradually increased. Notice that adjacent to the driven pile, it is common to find a gap or little heave between the pile shaft and the surrounding soil. The effect is probably due to friction between the pile shaft and the surrounding soil, which dragged down the soil close to the shaft during pile progressive penetration (Ni et al. 2010, Massarsch & Wersall 2013).

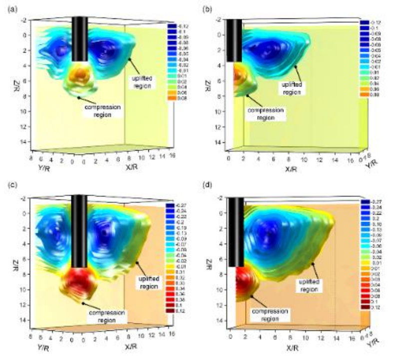

Figure 11 The different stages of vertical displacement isosurface for flat-ended pile penetration,δw/R: a front view, Z/R=3.5; b side view, Z/R=3.5; c front view, Z/R=7; d side view, Z/R=7.

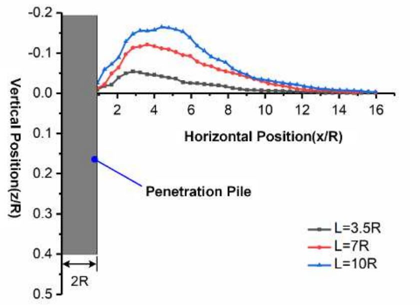

Figure 12 The ground heave of different stages for flat-ended pile, δw/R.

4 CONCLUSIONS

This study presented a novel automatic tomographic scanning measuring device and a modified 3D reconstruction procedure with the transparent soil model and incremental RG-PIV technique. They are used to investigate the penetration mechanisms and the disturbance effect for pile penetration quantitatively. The main conclusions obtained in this study are as follows:

(1) The overall layout of the novel automatic tomographic scanning measuring device is described in detail in this paper, and the principle of synchronization of the device is also introduced. The detailed steps of the modified 3D reconstruction technique are also explained. The modified 3D reconstruction procedure can intuitively plot 3D displacement field. It is worth noting that, the novel tomographic scanning measuring device is of versatility and relative affordability compared to other 3D measurement technology.

(2) One key mechanism was found to occur during pile penetration, namely, the displacement patterns are mainly divided into compression region and uplift region. In the case of the compression region, the pressurized bulb moves progressively downward as the pile penetrates into the ground; for the uplift region, the deformation of soil around the pile is mainly inclined upward for the so-called shallow penetration.

(4) The stages of lateral expansion can be roughly divided into two: when the pile tip contacted the soil, the soil disturbance around the pile tip will produce a compressive expansion effect; when the pile tip has passed, it has the effect of secondary accumulation expansion on the upper soil.

(5) Due to friction between the pile shaft and the surrounding soil, which dragged down the soil close to the shaft during pile progressive penetration. Accordingly, the variation trend of ground heave is roughly similar in different penetration stages, which increases first and then decreases.

5 REFERENCES

References in alphabetical order, using Times New Roman 8 point font.

Gibson R.E. and Henkel D.J. 1954. Influence of duration of tests at constant rate of strain on measured “drained” strength. *Géotechnique* 4 (1), 6-15.

Darcy H. 1856. *Les fontaines publiques de la ville de Dijon*. Dalmont, Paris.

Terzaghi K. 1936. The shearing resistance of saturated soils. *Proc. 1st Int. Conf. Soil Mech.*, Cambridge, Mass., 1, 54-56.

Chong M.K. 2013. Soil movements due to displacement pile driving, *Proc. 7th Int. Conf. on Case Histories in Geotechnical Engineering*, Paper No. 2.59, http://scholarsmine.mst.edu/icchge.

Cnudde V. and Boone M.N. 2013. High-resolution X-ray computed tomography in geosciences: A review of the current technology and applications. *Earth-Science Reviews*, 123, 1-17.

Cooke R., Price G., Tarr K. 1979. Jacked piles in London Clay: a study of load transfer and settlement under working conditions. *Geotechnique* 29 (2):113-147.

Cubes M. 1987. A high resolution 3D surface construction algorithm. *Proc. of the 14th Annual Conf. on Computer Graphics and Interactive Techniques*. New York: Association for Computing Machinery. 1987: 163-69.

De Cataldo D., Chen K., Airey D. 2017. Three-dimensional deformations in transparent soil using fluorescent markers. *International Journal of Physical Modelling in Geotechnics*, 17(2): 122-134.

Ezzein F.M. and Bathurst R.J. 2011. A transparent sand for geotechnical laboratory modeling. *Geotechnical Testing Journal*, 34(6): 590-601.

Garcia D., Orteu J.J., Penazzi L. 2002. A combined temporal tracking and stereo-correlation technique for accurate measurement of 3D displacements: application to sheet metal forming. *J Mater Process Technol* 125:736–742.

Guzman I.L. and Iskander M. 2013. Geotechnical properties of sucrose-saturated fused quartz for use in physical modeling. *Geotechnical Testing Journal*, 36(3): 448-454.

Guzman I.L., Iskander M., Suescun-Florez E., et al. 2014. A transparent aqueous-saturated sand surrogate for use in physical modeling. Acta Geotechnica, 9(2): 187-206.

Hall S.A., Bornert M., Desrues J., et al. 2010. Discrete and continuum analysis of localised deformation in sand using X-ray μCT and volumetric digital image correlation. *Géotechnique*, 60(5): 315-322.

Higo Y., Oka F., Sato T., et al. 2013. Investigation of localized deformation in partially saturated sand under triaxial compression using microfocus X-ray CT with digital image correlation. *Soils and Foundations*, 53(2): 181-198.

Hird C.C., Ni Q., Guymer I. 2011. Physical modelling of deformations around piling augers in clay. *Geotechnique*, 61(11): 993-999.

Hu P., Stanier S.A., Wang D., Cassidy M.J. 2015. Effect of footing shape on penetration in sand overlying clay. *International Journal of Physical Modelling in Geotechnics* 16 (3):119-133

Hwang J.-H., Liang N., Chen C.-H. 2001. Ground response during pile driving. *Journal of Geotechnical and Geoenvironmental Engineering*, 127 (11):939-949.

Iskander M.G., Sadek S., Liu J. 2002. Optical measurement of deformation using transparent silica gel to model sand. *International Journal of Physical Modelling in Geotechnics*, 2(4): 13-26.

Iskander M.G., Liu J. 2010. Spatial deformation measurement using transparent soil. *Geotechnical Testing Journal*, 33(4): 314-321.

Iskander M.G. 2010. *Modelling with transparent soils: Visualizing soil structure interaction and multi-phase flow, non-intrusively.* Springer Science & Business Media.

Iskander M.G., Bathurst R.J., Omidvar M. 2015. Past, present, and future of transparent soils. *Geotechnical Testing Journal*, 38(5): 557-573.

Kashuk S., Mercurio S.R., Iskander M.G. 2015. Methodology for optical imaging of NAPL 3D distribution in transparent porous media. *Geotech. Test. J.,* 38(5): 603-619.

Kobayashi T. and Fukagawa R. 2003. Characterization of deformation process of CPT using X-ray TV imaging technique. *3rd Int. Conf. on Deformation Characteristics of Geomaterials*, 43-47.

Kong G.Q., Cao Z.H., Zhou H., et al. 2015. Analysis of piles under oblique pullout load using transparent-soil models. *Geotechnical Testing Journal*, 38(5): 725-738.

Levoy M. 1988. Display of surfaces from volume data. *IEEE Computer graphics and Applications*, 8(3): 29-37.

Liu J. and Iskander M.G. 2010 Modelling capacity of transparent soil. *Canadian Geotechnical Journal*, 47(4): 451-460.

Losert W., Ronaszegi K., Weijs J., et al. 2009. Three dimensional particle rearrangements during slow granular shear flow in a split bottom geometry. *AIP Conference Proceedings. AIP,* 1145(1): 347-350.

Massarsch K.R. and Wersäll C. 2013. Cumulative lateral soil displacement due to pile driving in soft clay. *Geo-Congress 2013*; San Diego, California, United States March 3-7, 230, 463-480.

Pan B., Xie H., Guo Z., et al. 2007. Full-field strain measurement using a two-dimensional Savitzky-Golay digital differentiator in digital image correlation. *Optical Engineering*, 46(3): 033601.

Pan B., Xie H., Wang Z. 2010. Equivalence of digital image correlation criteria for pattern matching. *Applied optics*, 49(28): 5501-5509.

Pan B., Wand D., Yong X. 2012. Incremental calculation for large deformation measurement using reliability-guided digital image correlation. *Optics and Lasers in Engineering*, 50(4): 586-592.

Paniagua P., Andó E., Silva M., Emdal A., Nordal S., Viggiani G. 2013. Soil deformation around a penetrating cone in silt. *Géotechnique Letters*, 3 (4):185-191.

Randolph M.F., Wroth C.P. 2010. An analytical solution for the consolidation around a driven pile. *International Journal for Numerical & Analytical Methods in Geomechanics*, 3 (3):217-229.

Salgado R. and Prezzi M. 2007. Computation of cavity expansion pressure and penetration resistance in sands. *International Journal of Geomechanics,* 7(4): 251-265.

Sang Y., Wang Z., Yu S., et al. 2019. The Loading Test on the Singe Pile with Pile Cap in Transparent Soil Model. *Geotechnical Testing Journal,* 42(2): 385-406.

Sang Y, Zhao J, Duan F, et al. A novel automatic device to measure deformation inside transparent soil based on digital image correlation technology[J]. Measurement Science and Technology, 2019, 30(3).

Scarano F. 2012. Tomographic PIV: principles and practice. Measurement Science and Technology, 24(1): 012001.

Stanier S.A., Blaber J., Take W.A., et al. 2015. Improved image-based deformation measurement for geotechnical applications. *Canadian Geotechnical Journal*, 53(5): 727-739.

Toiya M., Hettinga J., Losert W. 2007. 3D Imaging of particle motion during penetrometer testing. Granular Matter, 9(5): 323-329.

Vanne J., Aho E., Hamalainen T.D., et al. 2006. A high-performance sum of absolute difference implementation for motion estimation. *IEEE Transactions on Circuits and Systems for Video Technology*, 16(7): 876-883.

Viggiani G., Andò E., Takano D., et al. 2014. Laboratory X-ray tomography: a valuable experimental tool for revealing processes in soils. *Geotechnical Testing Journal*, 38(1): 61-71.

White D.J. and Bolton M.D. 2004. Displacement and strain paths during plane-strain model pile installation in sand. *Géotechnique*, 54 (6):375-397.

Xiao Y., Yin F., Liu H., et al. 2016. Model tests on soil movement during the installation of piles in transparent granular soil. *International Journal of Geomechanics*, 17(4): 06016027.

Yetginer A.G., White D.J., Bolton M.D. 2006. Field measurements of the stiffness of jacked piles and pile groups. *Géotechnique*, 56(5): 349-354.

Yu L. and Pan B. 2017. Color stereo-digital image correlation method using a single 3CCD color camera. *Experimental Mechanics*, 57(4): 649-657.

Yuan B., Liu J., Chen W., et al. 2011. Development of a robust Stereo-PIV system for 3-D soil deformation measurement. *Journal of Testing and Evaluation*, 40(2): 256-264.

Yuan B., Chen R., Teng J., et al. 2015. Investigation on 3D ground deformation and response of active and passive piles in loose sand. *Environmental earth sciences*, 73(11): 7641-7649.

Zhang Q.C., Wang W.F., Zuo J.M., et al. 2014. CT image binarization threshold selection of coal and 3D reconstruction technology research. *CT Theory and Applications*, 23(1): 45-51.

Zhao H., Ge L., Luna R. 2010. Low viscosity pore fluid to manufacture transparent soil. *Geotechnical Testing Journal,* 33(6): 463-468.

Zhao H. and Ge L. 2014. Investigation on the shear moduli and damping ratios of silica gel. *Granular Matter*, 16(4): 449-456.

Zheng K.H. 2016. *Study on mesostructure and damage characteristics for coal and gangue particles based on X-ray* CT. PhD thesis, China University of Mining & Technology.